Earth Planet. Sci. Lett. 667 (2025) 119530

Contents lists available at ScienceDirect

Earth and Planetary Science Letters

journal homepage: www.elsevier.com/locate/epsl

The evolution of planetesimal reservoirs revealed by Fe-Ni isotope anomalies in differentiated meteorites

Fridolin Spitzer [a,b,*], Timo Hopp [a,c], Christoph Burkhardt [a,b], Nicolas Dauphas [c], Thorsten Kleine [a,b]

[a] Max Planck Institute for Solar System Research, Justus-von-Liebig-Weg 3 37077, Göttingen, Germany
[b] Institut für Planetologie, University of Münster, Wilhelm-Klemm-Str. 10 48149, Münster, Germany
[c] Origins Laboratory, Department of the Geophysical Sciences and Enrico Fermi Institute, The University of Chicago, Chicago 60637, USA

ARTICLE INFO

Editor: Dr O Mousis

Keywords:
Planetesimals
Carbonaceous chondrites
Iron meteorites
Accretion
Ni isotopes
Fe isotopes
CI chondrites

ABSTRACT

Differentiated meteorites sample planetesimals formed earlier than the parent bodies of chondritic meteorites. To evaluate whether these two generations of planetesimals formed from the same or distinct materials, we have analyzed the Fe and Ni isotopic compositions for a large set of differentiated meteorites, representing approximately 26 distinct parent bodies. Most of these samples are genetically related to the carbonaceous chondrite (CC)-type reservoir, which is thought to represent some portion of the outer disk. The new data reveal that early and late CC planetesimals cover a similar range of Fe and Ni isotopic compositions, indicating that all these bodies accreted from the same mixture of dust components, either in a long-lived pressure structure of the disk or in different substructures containing the same materials. Many differentiated meteorites have an isotopic composition similar to the late-formed CR chondrites, indicating that the CR chondrite reservoir was established early and remained isolated for essentially the entire disk lifetime. Finally, CI chondrites are the only CC chondrites whose isotopic composition is not represented among differentiated meteorites. Thus, planetesimals with CI chondrite-like isotopic compositions represent a late burst of planetesimal formation and possibly formed by a distinct mechanism and/ or in a different location from the other CC planetesimals.

1. Introduction

Planetesimals are gravitationally bound objects typically 1–500 km in size that are widely considered to represent the first planetary bodies to form in accretion disks around young stars (Blum, 2018). They are thought to have formed by streaming instabilities (SI) in the circumsolar disk at locations with a dust-to-gas ratio of about unity (Youdin and Goodman, 2005). Such increased dust-to-gas ratios can be achieved in dust drift barriers related to pressure maxima that form in the vicinity of growing planetary cores (Bitsch et al., 2018), or at the sublimation fronts of solids (Drążkowska and Alibert, 2017; Izidoro et al., 2022; Morbidelli et al., 2022).

In the solar system, planetesimal formation can be studied by analyzing meteorites, which derive from main belt asteroids and sample left-over planetesimals. Meteorites exhibit nucleosynthetic isotope anomalies, which arise from the heterogeneous distribution of presolar matter in the solar accretion disk. This makes these anomalies powerful tracers for identifying the formation location of individual objects and for establishing genetic links among distinct meteorite parent bodies. The nucleosynthetic isotope heterogeneity among meteorites has provided two key observations. First, there is a fundamental dichotomy between non-carbonaceous (NC) and carbonaceous (CC) meteorites, indicating that meteorite parent bodies formed in two spatially distinct reservoirs, which have been interpreted to represent the inner and outer disk, respectively, separated by the early formation of proto-Jupiter (Budde et al., 2016; Kruijer et al., 2017; Warren, 2011). In addition, the uniquely distinct Fe and Ni isotope composition of the Ivuna-type (CI) chondrites has been used to argue that these chondrites formed farther out in the disk (Hopp et al., 2022a; Spitzer et al., 2024), but as to whether they sample a third, spatially separated reservoir (Hopp et al., 2022a) is debated (Spitzer et al., 2024).

The second key observation is that both NC and CC are comprised of meteorites from early- and late-formed parent bodies (Kruijer et al., 2017). The former are represented by differentiated meteorites (achondrites and iron meteorites), which derive from parent bodies that accreted within the first ~1.5 million years (Ma) of the solar system

* Corresponding author.
E-mail address: spitzer@mps.mpg.de (F. Spitzer).

https://doi.org/10.1016/j.epsl.2025.119530
Received 20 March 2025; Received in revised form 23 June 2025; Accepted 25 June 2025
Available online 14 July 2025

(Kleine et al., 2005; Kruijer et al., 2014). The late-formed objects are the undifferentiated chondrite parent bodies, which accreted between ~2–4 Ma after solar system formation (Krot and Bizzarro, 2009). While the early-accreted bodies melted and chemically differentiated due to heating from decay of ^{26}Al, the later-formed chondrite parent bodies contained too little ^{26}Al to melt and differentiate (Hevey and Sanders, 2006; Kleine et al., 2005). As such, these bodies still contain some of the distinct dust components from which they accreted. For instance, carbonaceous chondrites contain variable abundances of chondrules (silicate spherules formed by melting of dust aggregates in the disk), refractory inclusions (high-temperature condensates thought to have formed close to the young Sun), Fe-Ni metal, and fine-grained matrix (a mixture of thermally processed and unprocessed dust, rich in volatile elements, organics, and presolar grains) (Scott and Krot, 2013). Some of these components formed at different times and different locations in the disk, and so their occurrence in the carbonaceous chondrites bears testimony to the transport and mixing of these materials in the disk. It has been suggested that the carbonaceous chondrites formed in a pressure bump located outside of proto-Jupiter's orbit, where the varying abundances of the distinct components reflect their different accretion efficiencies within this structure (Desch et al., 2018; Hellmann et al., 2023). This raises the question of whether the early-formed, differentiated CC planetesimals accreted from the same materials and in the same pressure bump as the later-formed carbonaceous chondrite parent bodies. Obtaining this information is of considerable interest, as it would help constrain the extent and efficiency of transport, mixing, and storage of different dust populations in the evolving solar accretion disk. Contrary to the chondrites, any primary textural information on the materials accreted into early planetesimals is lost due to their melting by heating from ^{26}Al-decay. However, information about the dust mixtures forming the first generation of planetesimals can be derived indirectly by comparing their nucleosynthetic isotope signatures to those of chondrites (Bryson and Brennecka, 2021).

The isotope anomalies in Fe and Ni are well-suited for assessing whether early- and late-formed CC-type meteorites formed from the same or different materials because NC and CC meteorites have distinct Fe and Ni isotopic compositions and because there are isotopic variations among carbonaceous chondrites and in particular CI chondrites and samples returned from the Cb-type asteroid Ryugu by the Hayabusa2 mission have Fe and Ni isotopic compositions well resolved from any other carbonaceous chondrite (Hopp et al., 2022a; Spitzer et al., 2024). Moreover, as siderophile elements, Fe and Ni are abundant in iron meteorites and so their isotopic compositions can readily be analyzed in these samples. This is important because iron meteorites constitute the largest set of differentiated meteorites and derive from a large number of distinct parent bodies (Goldstein et al., 2009; Spitzer et al., 2025). Here, we present new Fe and Ni isotopic data for iron meteorites and achondrites derived from ~26 different early-formed bodies. These data are used to quantify the extent of Fe and Ni isotopic variability among CC-type meteorites and to assess whether this variability is different for early- and late-formed objects in the CC reservoir. Together, the new data provide important constraints for understanding planetesimal formation in the outer disk, including the unique process that formed CI chondrite-like objects.

2. Samples and methods

This study is focused on ungrouped iron meteorites. These do not appear to be directly related to any of the 13 major iron meteorite groups and likely represent the only known samples of their parent bodies. Thus, by analyzing ungrouped iron meteorites, the isotopic signatures for a large number of parent bodies can be obtained. Previous Fe and Ni isotope studies have largely focused on the major iron meteorite groups, and so the Fe and Ni isotope systematics of ungrouped irons have until now remained unexplored. For this study, 27 ungrouped irons were selected. All these samples were already characterized for their Mo isotope signatures (defining their genetic association to either NC or CC) and ^{182}Hf-^{182}W core formation chronology (Spitzer et al., 2025). Collectively, these data show that 9 of the ungrouped irons are NC and 17 are CC (Spitzer et al., 2025). Most ungrouped CC irons have Hf-W core formation model ages of ~3 Ma after solar system formation, indicating that these samples derive from objects that accreted within ≤1 Ma of solar system formation (Spitzer et al., 2025). Thus, all these samples derive from parent bodies that formed much earlier than the CC chondrites, which have parent body accretion ages of ~2–4 Ma after solar system formation (Krot and Bizzarro, 2009). In addition to the ungrouped irons, samples from the IIC, IIF, IIIE, IIIF, and IVB iron meteorite groups (all CC-type except for group IIIE) were also included in this study because for some of these groups, no, or only very few Fe and Ni isotopic data were available. Finally, four ungrouped CC achondrites were analyzed, for which CI chondrite-like ^{50}Ti or ^{54}Cr isotopic compositions were reported (Ma et al., 2022; Sanborn et al., 2019; Williams et al., 2020).

The sample preparation and chemical separation of Fe and Ni followed our previously established protocols (Hopp et al. 2022a,b; Spitzer et al. 2022, 2024). The isotopic compositions were measured at the University of Münster, the University of Chicago, and the Max Planck Institute for Solar System Research, Göttingen, using a ThermoScientific Neptune *Plus* (Chicago, Münster) or Neoma MC-ICP-MS (Göttingen), and are reported in the μ-notation, which is the parts-per-million deviation from the terrestrial standard after mass-bias correction to ^{61}Ni/^{58}Ni, ^{62}Ni/^{61}Ni, or ^{57}Fe/^{56}Fe, using the exponential law. Planetary and nebular processes are expected to follow mass-dependent isotopic fractionation, so all materials derived from the same homogeneous reservoir are expected to have identical μ-values. Iron meteorites tend to have long cosmic ray exposure (CRE) ages of up to one billion years (Herzog and Caffee, 2014) and, therefore, it is necessary to quantify potential secondary modifications of the original isotopic composition due CRE-induced secondary neutron capture effects. Such CRE effects can be corrected by also measuring Pt isotopic compositions in the same samples, which serve as an in-situ neutron dosimeter (Kruijer et al., 2013; Wittig et al., 2013). Previous studies showed that Ni isotopes are not significantly affected by CRE and, thus, do not require any correction (Anand et al., 2024; Cook et al., 2020). However, the Fe isotope compositions of iron meteorites are modified during CRE and therefore require correction (Cook et al., 2020; Hopp et al., 2022b). For this correction, we use the Pt isotope compositions of the same samples and the empirically determined μ^{i}Fe-μ^{196}Pt slopes, where *i* stands for 54 or 58, respectively (Hopp et al., 2022b). The Pt isotopic compositions of the ungrouped irons of this study are from Spitzer et al. (2025), whereas those for samples of the IIC, IIF, IIIE, and IIIF groups are from this study.

The chemical purification of Pt followed our previously established protocols (Kruijer et al., 2014, 2013; Spitzer et al., 2025), and Pt isotope compositions were measured on the Neoma MS/MS MC-ICP-MS at the Max Planck Institute for Solar System Research in Göttingen. Platinum was introduced into the mass spectrometer using an Apex 2 IR at an uptake rate of ~70µl/min. The MS/MS was set to transmission mode (i.e., slid 100 % open) using an E-field of 43.3 V and a B-field of 10 %. Sample solutions were measured at 100 ppb, resulting in signal intensities of ~6 V on ^{195}Pt. One measurement consisted of 100 repeats of 4 s each. Instrumental mass bias was corrected relative to ^{198}Pt/^{195}Pt (0.2145) or ^{196}Pt/^{195}Pt (0.7464) using the exponential law. Os/Pt ratios of the samples were $\leq 2.4 \times 10^{-4}$ and, thus, within the range where isobaric interferences of ^{192}Os on ^{192}Pt can be accurately corrected (Kruijer et al., 2013). For most samples, significant amounts of Ir remained in the final Pt cuts, causing tailing effects on ^{192}Pt and ^{194}Pt from ^{191}Ir and ^{193}Ir, respectively, which were monitored and corrected by repeated measurements of Ir-doped Pt solution standards during each session (Kruijer et al., 2013). The accuracy and precision of the new measurement routine have been tested by re-measuring the purified Pt cuts of the ungrouped iron Reed City from Spitzer et al. (2025) and by measuring the NIST SRM 129c doped with Pt and other Pt-group metals

(Alfa Aesar®) (Tables A2-3).

3. Results

The new Ni and Fe isotopic data are reported in Tables 1 and A1. The new Pt isotopic data used to correct for any CRE effects are reported in Table 2. All samples of this study plot in either the NC or CC fields as previously defined based on analyses of the different meteorite groups (Fig. 1). Importantly, the association of the ungrouped irons to either NC or CC is consistent with the genetics of these samples inferred from their Mo isotope signatures (Spitzer et al., 2025). The ungrouped irons display more scatter compared to the compositions of the iron meteorite groups, which, at least in part, reflects the larger associated uncertainties of the individual ungrouped irons compared to the well-defined means of the iron groups which are based on analyses of several individual samples.

Although the Fe and Ni isotopic compositions show little variations within the NC and CC reservoirs, two observations stand out. First, the isotopic compositions of CI chondrites and Ryugu are unmatched by any

Table 1
Fe and Ni isotopic compositions of differentiated meteorites.

ID	Sample	Type	N[a]	μ^{60}Ni	2 s.e.	μ^{62}Ni	2 s.e.	μ^{64}Ni	2 s.e.	N[a]	$\mu^{54}Fe_{corr.}$[b]	2 s.e.	$\mu^{58}Fe_{corr.}$[b]	2 s.e.
Non-carbonaceous meteorites														
MPS-38	Burlington	IIIE								15[e]	11	6	−18	10
MPS-39	Paneth's iron	IIIE								15[e]	7	7	−1	7
MPS-40	Coopertown	IIIE								30[e]	7	7	−5	8
UI-02	Butler	Iron ungr.	12[d]	−8	4	−11	8	−38	12	15[f]	11	8	−7	8
UI-03	Cambria	Iron ungr.	16[d]	−6	4	−9	8	−30	14	15[f]	7	7	−6	13
UI-07	Reed City	Iron ungr.	23[e]	−4	2	−6	5	−22	10	15[f]	14	7	−4	15
UI-09	Zacatecas (1792)	Iron ungr.	15[d]	−8	3	−11	8	−27	17	15[f]	13	5	−5	9
UI-10	Guin	Iron ungr.	16[d]	−4	4	2	8	−3	19	15[f]	7	7	0	15
UI-15	Santiago Papasquiero	Iron ungr.	24[e]	−6	3	−4	5	−11	7	15[f]	11	4	−2	8
UI-17	Washington County	Iron ungr.	20[d]	−6	3	−5	5	−21	12	15[f]	12	6	−6	11
UI-19	EET 83230	Iron ungr.	16[d]	−11	3	−8	6	−14	11	15[f]	11	6	6	12
UI-26	NWA 859	Iron ungr.	15[d]	−9	4	−11	7	−27	12	15[f]	11	5	−14	11
Carbonaceous meteorites														
AD03–1	Skookum	IVB	26[d,e]	−17	3	8	6	30	14					
AD03–2	Skookum	IVB	28[d]	−11	2	15	5	36	11					
AD03–3	Skookum	IVB	52[d,e]	−14	2	7	3	19	6					
AD03–4	Skookum	IVB	24[d]	−15	3	9	7	29	11					
GeA41	Unter-Mässing	IIC	20[e]	−17	3	12	5	41	10	15[e]	34	8	13	17
GeA49	Kumerina	IIC	16[e]	−17	3	15	5	45	8	15[e]	29	7	5	14
GeA40	Corowa	IIF	16[e]	−11	3	1	4	9	7	15[e]	30	6	1	12
GeA50	Balambala	IIF	16[e]	−9	2	2	6	7	10	15[e]	18	8	−5	15
AG04	Moonbi	IIIF	15[e]	−9	3	11	4	22	9	15[e]	17	8	4	9
AG05	St. Genevieve County	IIIF	16[e]	−10	2	3	5	9	7	15[e]	24	6	−4	10
UI-01	Babb's Mill (Troost's Iron)	Iron ungr. (SBT)	16[d]	−12	3	6	7	9	19	15[f]	25	5	0	15
UI-04	Grand Rapids	Iron ungr.	22[e]	−10	2	5	6	12	9	15[f]	29	7	−1	9
UI-06	Pinon	Iron ungr.	15[e]	−11	3	4	5	17	10	15[f]	21	4	9	13
UI-08	Tucson	Iron ungr.	12[d]	−12	5	7	10	19	19	15[f]	17	5	8	13
UI-11	Mbosi	Iron ungr.	14[d]	−14	6	6	10	8	16	15[f]	20	4	3	16
UI-12	New Baltimore	Iron ungr.	12[e]	−16	2	17	7	44	9	15[f]	24	7	10	16
UI-13	Nordheim	Iron ungr.	12[d]	−18	4	10	6	30	17	15[f]	38	5	0	11
UI-14	NWA 6932	Iron ungr.	24[e]	−10	3	8	4	12	7	15[f]	26	7	−4	12
UI-16	Tishomingo	Iron ungr.	12[d]	−18	3	9	6	32	12	15[f]	30	7	8	10
UI-18	ALHA 77255	Iron ungr.	16[d]	−21	4	9	6	31	16	15[f]	29	8	4	9
UI-20	Guffey	Iron ungr.	15[d]	−20	3	11	8	30	15	15[f]	29	7	5	14
UI-21	Hammond	Iron ungr.	15[e]	−16	3	17	5	48	10	15[f]	41	7	5	8
UI-22	ILD 83500	Iron ungr. (SBT)	16[e]	−11	3	10	5	19	8	15[f]	26	7	4	14
UI-23	Illinois Gulch	Iron ungr.	18[e]	−14	3	16	6	41	11	15[f]	40	5	2	11
UI-24	La Caille	Iron ungr.	20[e]	−19	3	12	6	36	9	15[f]	29	7	11	11
UI-25	N'Goureyma	Iron ungr.	12[e]	−14	2	15	3	41	13	15[f]	35	7	10	9
AD01	Chinga	Iron ungr.	21[d]	−17	3	7	4	21	12					
DI28	NWA 6926	Achondrite ungr.	13[e]	−18	2	10	4	30	8	15[e]	41	6	−1	7
AG02	NWA 6704	Achondrite ungr.	20[e]	−15	2	7	5	22	10	14[e]	34	6	10	9
AG01	Tafassasset metal	Achondrite ungr.	16[e]	−19	2	10	3	32	6	15[e]	32	5	3	11
DI53	NWA 8548	Achondrite ungr.	17[e]	−13	2	10	3	31	8	15[e]	23	7	−1	11
Mixed NC-CC composition														
UI-05	Nedagolla[c]	Iron ungr.	20[d]	0	3	9	4	22	9	12[f]	−4	4	13	16
UI-05c	Nedagolla[c]	Iron ungr.	19[d]	1	3	10	8	12	13	12[f]	1	14	−8	13

Notes. All data are reported in the μ-notation (i.e. parts-per-million deviations from terrestrial standard values) after mass-bias correction to the terrestrial $^{61}Ni/^{58}Ni$ (= 0.016744) and $^{57}Fe/^{56}Fe$ (= 0.023095) using the exponential law. Reported μ-values represent the mean of N pooled solution replicates, and uncertainties are reported as two standard errors (2 s.e.). Babb's Mill (Troost's Iron) and ILD 83500 belong to the South Byron Trio and likely derive from the same parent body (SBT; Hilton et al., 2019).

[a] Number of measurements.

[b] The measured values have been corrected for CRE effects using the Pt isotopic composition measured for the same digestion from this study and Spitzer et al. (2025) and the empirically determined weighted mean $\mu^{i}Fe$-$\mu^{196}Pt$ slopes from IC and IIAB iron meteorites (Hopp et al., 2022b). This correction also takes a small nucleosynthetic anomaly on $\mu^{196}Pt$ into account (Spitzer et al., 2021). The associated uncertainties induced through this correction were propagated into the final reported uncertainties of the Fe isotope ratios.

[c] Ni isotope data as reported by Spitzer et al. (2022).

[d] Data were obtained using the Neptune MC-ICP-MS at the University of Münster.

[e] Data were obtained using the Neoma MC-ICP-MS at the Max Planck Institute for Solar System Research in Göttingen.

[f] Data were obtained using the Neptune MC-ICP-MS at the University of Chicago.

Table 2
Pt isotopic compositions of grouped iron meteorites.

ID	Sample	Type	N[a]	$\varepsilon^{192}Pt_{(6/5)}$	(± 2σ)	$\varepsilon^{194}Pt_{(6/5)}$	(± 2σ)	$\varepsilon^{198}Pt_{(6/5)}$	(± 2σ)	$\varepsilon^{192}Pt_{(8/5)}$	(± 2σ)	$\varepsilon^{194}Pt_{(8/5)}$	(± 2σ)	$\varepsilon^{196}Pt_{(8/5)}$	(± 2σ)
GeA41	Kumerina	IIC	2	0.82	0.73	−0.05	0.15	−0.01	0.24	0.81	0.86	−0.05	0.10	0.00	0.08
GeA49	Unter-Mässing	IIC	1	6.44	0.73	0.35	0.15	−0.42	0.24	6.02	0.86	0.21	0.10	0.14	0.08
GeA40	Corowa	IIF	2	3.96	0.73	0.35	0.15	−0.69	0.24	3.27	0.86	0.12	0.10	0.23	0.08
GeA50	Balambala	IIF	2	17.15	0.73	1.38	0.15	−2.05	0.24	15.10	0.86	0.69	0.10	0.68	0.08
AG04	Moonbi	IIIF	4	5.59	0.56	1.50	0.17	−1.81	0.16	3.78	0.50	0.90	0.13	0.60	0.05
AG05	St. Genevieve County	IIIF	4	7.65	0.67	0.69	0.11	−1.13	0.11	6.52	0.57	0.31	0.08	0.38	0.04
MPS-38	Burlington	IIIE	5	0.29	0.53	0.13	0.23	−0.33	0.36	−0.04	0.21	0.03	0.11	0.11	0.12
MPS-39	Paneth's Iron	IIIE	5	0.70	0.28	0.21	0.09	−0.39	0.13	0.32	0.21	0.09	0.05	0.13	0.04
MPS-40	Coopertown	IIIE	7	0.09	0.31	−0.04	0.05	−0.08	0.18	0.01	0.37	−0.06	0.03	0.03	0.06

All data are reported in the ε-notation (i.e., parts-per-10^4 deviations from terrestrial standard values) after mass-bias correction to $^{198}Pt/^{195}Pt = 0.2145$ (8/5) or $^{196}Pt/^{195}Pt = 0.7464$ (6/5) using the exponential law. For samples analyzed several times, reported ε-values represent the mean of pooled solution replicates, and uncertainties are reported as two standard errors (2 s.d.) for $N < 4$ based on the external reproducibility or as student-t 95 % confidence intervals (95 % CI) for $N \geq 4$.
[a] Number of measurements.

of the iron meteorites and achondrites (Fig. 1 and 2). Second, the CR chondrites have the highest $\mu^{54}Fe$ and $\mu^{60}Ni$ values, different from all other carbonaceous chondrites. But unlike CI chondrites, this composition is found in many (~50 %) of the ungrouped CC irons of this study, indicating that the specific CR chondrite-like isotopic composition is prevalent among differentiated meteorites. This also includes three of the ungrouped achondrites of this study, whose Fe and Ni isotopic compositions most closely resemble those of the metal-rich carbonaceous chondrites (CR, CH, CB) but are distinct from CI chondrites (Fig. 2 and 3). Thus, although these samples have similar ^{50}Ti and ^{54}Cr isotopic compositions as CI chondrites, the Fe and Ni isotopic data indicate they are not genetically related. This multimodality of meteorite isotopic anomalies is most clearly visible in $\mu^{54}Fe$-$\mu^{60}Ni$ isotope space (Fig. 3), where CI chondrites/Ryugu and the other CC meteorites seem to fall into three distinct clusters. A k-means clustering algorithm confirms the presence of three statistically significant clusters based on the elbow method and silhouette analysis. The CI-, CC-, and CR-clusters determined in this way are highlighted in Fig. 3.

4. Discussion

Two key observations can be made from the new Fe and Ni isotopic data. First, the Fe and Ni isotopic compositions of CI chondrites and Ryugu are not matched by any of the differentiated meteorites. Given that data are now available for ~26 early-formed CC objects, it is unlikely that the absence of CI-chondritic Fe and Ni isotopic compositions among these bodies reflects a sampling bias (cf. Yap and Tissot 2023). This in turn implies that planetesimals with the specific CI-chondritic Fe and Ni isotopic composition did not differentiate. Second, with the sole exception of the CI chondrites/Ryugu, early- and late-formed planetesimals (i.e., parent bodies of differentiated meteorites and chondrites, respectively) from both the NC and CC reservoirs cover the same range of isotope anomalies. This implies that in each reservoir, early- and late-formed planetesimals formed from similar mixtures of dust components having the same or similar isotopic compositions. These two observations combined provide essential information on the nature of planetesimal formation in the solar system and on the lifetime of distinct dust components in the disk.

4.1. Formation of early and late planetesimals from the same dust components

As noted above, isotopic variations among CC chondrites have been attributed to variable mixing among chondrules, refractory inclusions [Ca-Al-rich inclusions (CAIs) and amoeboid olivine aggregates (AOAs)], and matrix, all having distinct isotopic compositions (Alexander, 2019; Hellmann et al., 2023). The success of this mixing model is reflected in two main observations. First, the isotopic variations among the CC chondrites correlate with the inferred matrix mass fraction of each chondrite, demonstrating that a CC chondrite's isotopic composition systematically varies with the relative abundances of its constituent components. Second, the isotopic variations among the CC chondrites can be quantitatively reproduced using the observed isotopic compositions of refractory inclusions, chondrules, and CI-like matrix (Alexander, 2019; Hellmann et al., 2023). This mixing model is predominantly based on isotopic anomalies in (mostly) lithophile elements (i.e., $\Delta^{17}O$, ^{50}Ti, ^{54}Cr) together with elemental and mass-dependent isotopic variations in moderately volatile elements (e.g., Te, Zn, Rb, K, Ge) (Hellmann et al., 2020; Nie et al., 2021; Pringle et al., 2017; Wölfer et al., 2025). However, this model cannot easily account for the observed Fe and Ni isotope varations, because CI chondrites, which are almost pure matrix, have different isotopic anomalies than the matrix of other carbonaceous chondrites as inferred indirectly using correlations of Ni isotopic compositions with ^{50}Ti and ^{54}Cr isotope anomalies and matrix mass fractions (Spitzer et al., 2024). To account for these observations, Spitzer et al. (2024) argued that the isotopic difference between CI and the CC chondrites reflects that all non-CI chondrites lost a small fraction of isotopically anomalous FeNi metal grains.

If the isotopic variations among all CC chondrites (except CI) reflect mixing of the same components, then the similar ranges of Fe and Ni isotopic compositions of differentiated and chondritic CC meteorites imply that they all formed from similar mixtures of these components. The variable abundances of components among the CC chondrites is thought to reflect their formation in a pressure trap in the disk, possibly located just outside Jupiter's orbit, where the accretion efficiencies of the individual dust components varied over time due to their distinct aerodynamic properties (Desch et al., 2018; Hellmann et al., 2023). For instance, during a streaming instability, particles with higher Stokes numbers (i.e., the largest and densest grains) are preferentially incorporated into the growing planetesimals (Bai and Stone, 2010), depleting the reservoir in these components. Thus, planetesimals formed in consecutive phases of streaming instabilities would have incorporated different proportions of these components. This is consistent with the observation that earlier-formed CC chondrites (e.g., CV, CO chondrites) are richer in refractory inclusions and chondrules than their later-formed counterparts (e.g., CM chondrites) (Hellmann et al., 2023). Consquently, our finding that the parent bodies of differentiated CC meteorites formed from the same principal components as the CC chondrites implies that these components were already present in the CC region of the disk within one Ma after CAI formation (the inferred accretion age of the CC irons), and that the fractionation among these components during parent body accretion occurred similarly. Thus, the accretion process of early- and late-formed CC parent bodies was similar, because otherwise the range of Fe and Ni isotopic compositions among early- and late-formed CC meteorites would not be expected to be similar.

Refractory inclusions (CAIs and AOAs) are thought to have formed in a short time interval close to the young Sun and were subsequently

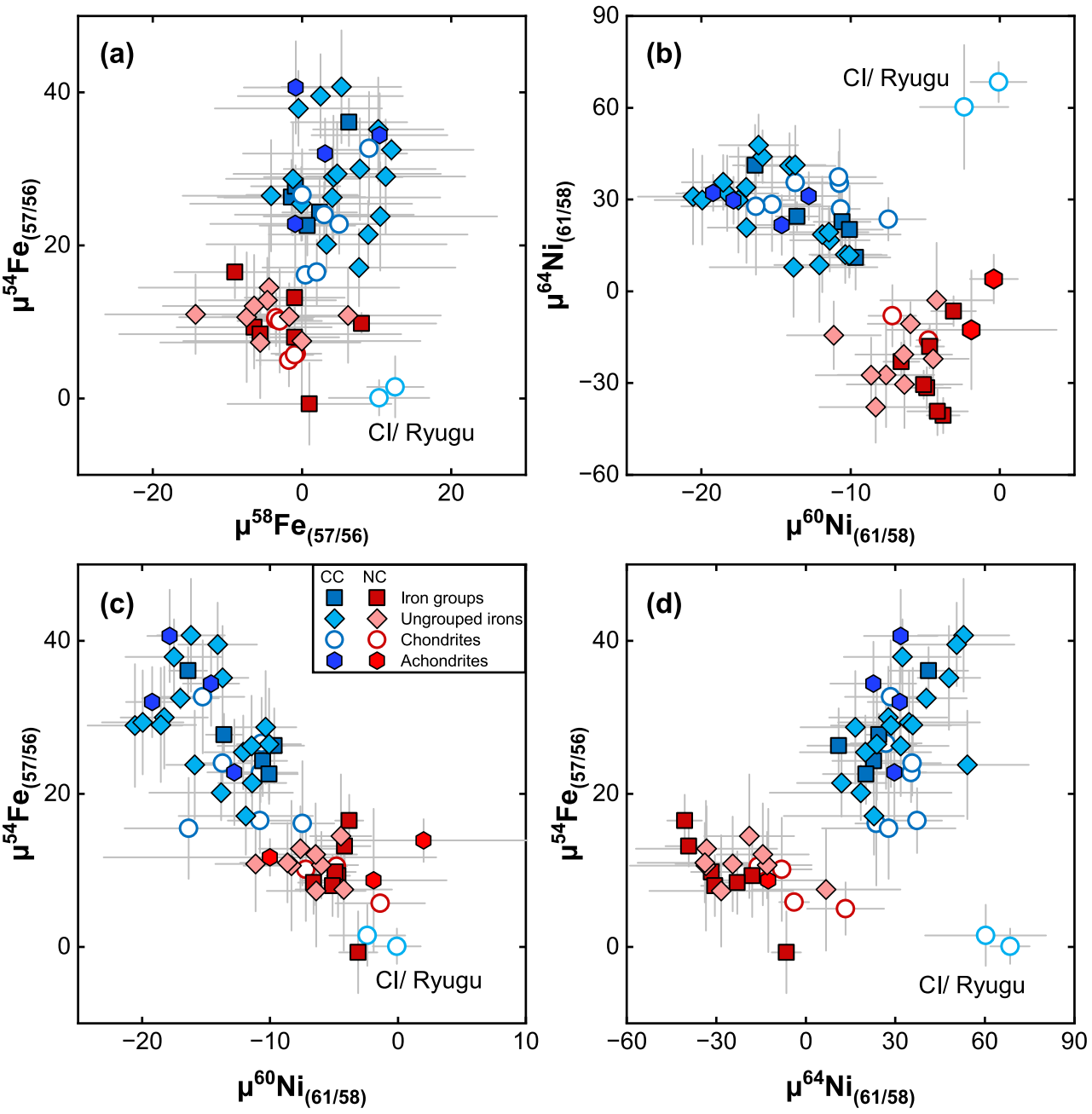

Fig. 1. Combined Fe and Ni isotopic compositions of differentiated and undifferentiated meteorites. The anomalies of the ungrouped iron meteorites overlap with those of the major magmatic iron meteorite groups and adhere to the NC and CC clustering (a–d). In $\mu^{54}Fe$–$\mu^{60}Ni$ space, all meteorites define a negative correlation with a slope of ~ –2 (c; Spitzer et al., 2024). The unique isotopic signature of Ryugu is best illustrated when $\mu^{54}Fe$ or $\mu^{60}Ni$ is plotted against $\mu^{64}Ni$ (b, d). Fe and Ni literature data as compiled in Hopp et al. (2022a) and Spitzer et al. (2024) with additions from Anand et al. (2024).

transported to the outer disk, from where they drifted back towards the Sun (Ciesla, 2007; Desch et al., 2018; Yang and Ciesla, 2012). As such, their occurrence in the relatively late-formed CC chondrites is attributed to accumulation in a dust drift barrier, which may had formed just outside of proto-Jupiter's core (Desch et al., 2018; Hellmann et al., 2023; Yang and Ciesla, 2012). Models of disk evolution show that some pile-up of refractory inclusions in such a structure may have already occurred early, within <1.5 Ma after their formation (see Fig. 8 in Desch et al., 2018), and so it is conceivable that these refractory inclusions were already available for accretion into the early-formed CC parent bodies. By contrast, the vast majority of chondrules are thought to have formed more than ~2 Ma after solar system formation and, thus, after accretion of the parent bodies of the differentiated CCs (e.g., Marrocchi et al., 2024). The rare occurrence of chondrules with older inferred formation ages (Bollard et al., 2017; Connelly et al., 2012; Piralla et al., 2023; Villeneuve et al., 2009), and the identification of relict chondrules in some primitive achondrites (Ma et al., 2022; Tomkins et al., 2020) suggest that there might have been an earlier generation of chondrules that was incorporated into the differentiated CC parent bodies. Nevertheless, the nucleosynthetic isotope signatures would be the same for chondrules and their precursors because these signatures do not change during the melting that produced the chondrules. Thus, our finding that early- and late-formed CC parent bodies incorporated similar mixtures of components only requires that the precursor dust of chondrules, and not chondrules themselves, were present during the accretion of the early CC bodies. This is consistent with the expectation that chondrule

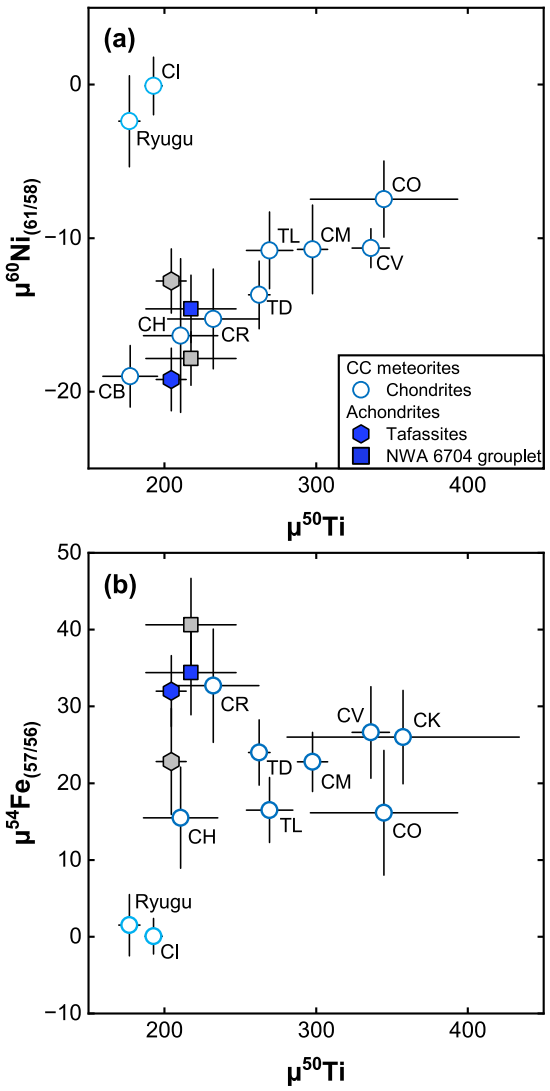

Fig. 2. Diagrams of $\mu^{60}Ni_{61/58}$ (a) and $\mu^{54}Fe_{57/56}$ (b) versus $\mu^{50}Ti$ for CC meteorites, respectively. Although some CC achondrites display CI-like Ti (and Cr) isotopic compositions, they are distinct from CI chondrites concerning their Fe and Ni isotopic compositions. This illustrates the unique Ni and Fe isotopic composition of CI chondrites and Ryugu samples. No published Ti data are available for NWA 6926 and NWA 8548 (grey data points), which is why we plot the Ti data of NWA 6704 and Tafassasset, respectively, because they were proposed to be genetically related (Ma et al., 2022). TD – Tarda. TL – Tagish Lake.

precursors consist of dust aggregates which themselves formed by the accumulation of early condensates, including refractory inclusions and dust grains that condensed at lower temperatures (Marrocchi et al., 2024).

Altogether, these observations imply that the first generation (differentiated meteorites) and second generation (chondrites) of CC planetesimals formed either in the same long-lived pressure structure of the disk or in different substructures that contained the same dust components. The former might require replenishment of CAIs from some other area of the disk after the formation of the iron meteorite parent bodies ceased (and consumed most of the available CAIs) and before the recurrent onset of CC chondrite formation. Preservation of the dust components that formed CC bodies over an extended period (i.e., up until ~4 Ma after CAI formation, the accretion time of the CR chondrites) demonstrates that there must have been an efficient dust drift barrier that prevented the loss of these components into the Sun. This is

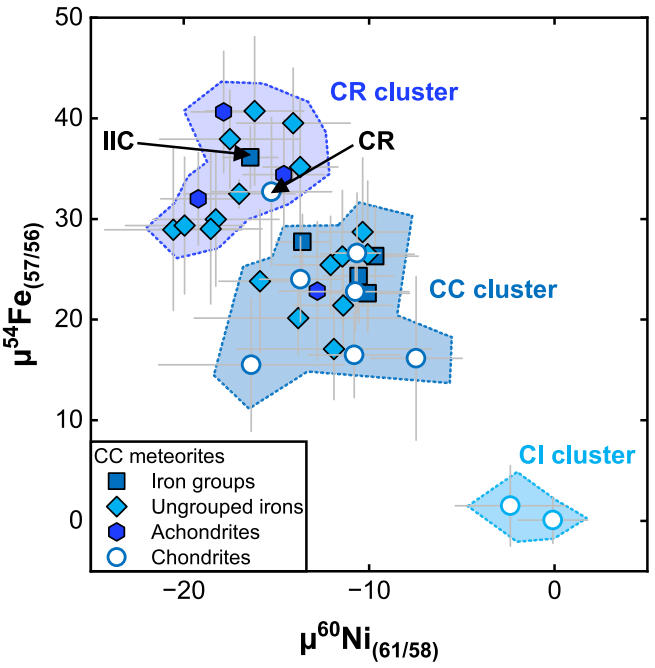

Fig. 3. Diagram of $\mu^{54}Fe_{57/56}$ vs. $\mu^{60}Ni_{61/58}$ for CC meteorites. The combined Fe-Ni isotope systematics highlight the unique isotopic signature of CI chondrites and Ryugu samples. Furthermore, ~50 % of the ungrouped iron meteorites, as well as the investigated ungrouped achondrites (except NWA 8548), display Fe-Ni isotopic compositions overlapping with those of CR chondrites and IIC iron meteorites.

consistent with the effective isolation of the NC reservoir, which is located closer to the Sun, from contamination with inward drifting CC dust from the outer disk (Budde et al., 2016; Burkhardt et al., 2021; Dauphas et al., 2024; Hopp et al., 2022b; Kruijer et al., 2017; Spitzer et al., 2020; Warren, 2011; Yap and Tissot, 2023).

4.2. *Early formation of CR planetesimals in a distinct outer region of the disk*

The CR chondrites, like the CI chondrites, formed relatively late, at ~4 Ma after CAI formation (Budde et al., 2018; Schrader et al., 2017). Several of the differentiated CC meteorites of this study have Fe and Ni isotopic compositions similar to the CR chondrites, indicating that planetesimals with a CR chondrite-like isotopic composition already formed early. Of note, about half of the ungrouped CC irons of this study are isotopically similar to CR chondrites (Fig. 3). This is different from the CC iron meteorite groups, which except for the IIC irons are isotopically distinct from CR chondrites (Fig. 3). Thus, a substantial number of early-formed objects are genetically related to the CR chondrites. This is consistent with the results of Ma et al. (2022), who argued on petrological, isotopic, and chronological grounds that some ungrouped primitive achondrites (which they collectively termed Tafassites) are genetically related to the CR chondrites but derive from objects that accreted earlier than these chondrites. Consistent with this, three of the four ungrouped achondrites of this study have Fe and Ni isotopic compositions indistinguishable from those of the CR chondrites (Fig. 2).

Among the CC chondrites, the CR chondrites stand out by several notable features. First, their nucleosynthetic ^{50}Ti and ^{54}Cr signatures are similar to those of the CI chondrites, yet unlike the CI chondrites, they are relatively poor in matrix. As a result, the CR chondrites are the only CC chondrites not plotting on the correlations between ^{50}Ti and ^{54}Cr anomalies and matrix mass fraction (Marrocchi et al. 2022). This has been attributed to the distinct isotopic compositions of CR chondrules, which have more elevated $\mu^{54}Cr$ values than chondrules from the CV,

CO, and CM chondrites (see Table A2 in Hellmann et al., 2023). Based on the textural and isotopic characterization of type I CR chondrules, it has been proposed that large CR chondrules formed by re-melting of pre-existing CM-CV-CO-like chondrules and during this event incorporated CI-like dust, implying that the original CR reservoir contained more matrix (~70–80 vol. %) than presently found in most CR chondrites (Bryson and Brennecka, 2021; Marrocchi et al., 2022). The presence of differentiated CR-like parent bodies, therefore, implies either that matrix-rich planetesimals already formed early or that chondrules (or their precursors) with a CR chondrite-like isotopic composition already existed earlier. Either way, the observation that in Fe-Ni isotope space the CR chondrites (and related differentiated meteorites) plot furthest away from CI chondrites indicates that the matrix in the CR chondrites is distinct from CI chondrites and may represent the matrix accreted by the non-CI carbonaceous chondrites.

Second, CR chondrites display low modal abundances of CAIs (0.6 vol.%), consistent with their CI-like Ti isotopic compositions (Fig. 2; Hellmann et al., 2023; Ma et al., 2022; Sanborn et al., 2019; Williams et al., 2020), and their low Δ^{95}Mo values—indicative of a relative deficit in *r*-process-derived nuclides (Budde et al., 2018; Wölfer et al., 2023)—that extend to CR-related achondrites (Budde et al., 2019), and the CR-like iron meteorites (Spitzer et al., 2025). The existence of early- and late-formed bodies with CR-like isotopic compositions, therefore, indicates the presence of a long-lived reservoir poor in refractory inclusions (Fig. A1), in contrast to other non-CI carbonaceous chondrites, in most of which refractory inclusions constitute an important component.

Third, bulk CR chondrites and CR chondrules are characterized by ^{26}Mg deficits (Luu et al., 2019; Van Kooten et al., 2024, 2016), which either reflects formation from materials poor in the parent radionuclide ^{26}Al or, as for ^{54}Cr, is due to a different nucleosynthetic make-up of CR compared to other chondrules (e.g., Olsen et al., 2016). For instance, it has been suggested that CR chondrites formed in a spatially separated reservoir beyond the orbit of Saturn and that their Mg isotope signatures reflect addition of pristine, ^{26}Al-poor material originating from the outermost disk (i.e., the comet-forming region) by late accretion streamers ~2–3 Ma after CAI formation (Van Kooten et al., 2024, 2020). However, this model is inconsistent with our finding of an early planetesimal population genetically related to the CR chondrites. First, since these data indicate that the isotopic composition of the CR chondrite reservoir was established early, it cannot simply reflect the addition of fresh material by late streamers to the outer disk. Second, the abundant presence of differentiated objects within the CR chondrite reservoir indicates that this reservoir initially cannot have been ^{26}Al-poor. This is because the decay of ^{26}Al is the only viable heat source for melting planetesimals, indicating that the CR planetesimals must have contained an appreciable amount of ^{26}Al. This is consistent with the good agreement among Al-Mg, Hf-W, and Pb-Pb ages of CR chondrites, which strongly argue for a homogeneous distribution of ^{26}Al throughout the disk, and including the CR chondrite reservoir (Budde et al., 2018).

In summary, the presence of differentiated bodies with CR chondrite-like isotope signatures indicates that despite the late formation time of the CR chondrites, a disk reservoir having a CR chondrite-like isotopic composition was established early and remained isolated until accretion of the CR chondrite parent body at ~3.7 Ma after CAI formation (Budde et al., 2018; Schrader et al., 2017) and thus for essentially the entire ~4 Ma lifetime of the disk (Wang et al., 2017). This reservoir was poor in refractory inclusions (<1 vol. %), contained matrix distinct from CI chondrites but similar to the matrix in other non-CI carbonaceous chondrites, and contained chondrules (or their precursors) with a distinct isotopic composition from chondrules in other carbonaceous chondrites. The characteristic ^{15}N and deuterium enrichments of the CR chondrites suggest that this reservoir was located at a greater heliocentric distance than those of most other carbonaceous chondrites (Alexander et al., 2012; Füri and Marty, 2015; Piani et al., 2021). However, the exact location of this reservoir and whether it was originally located beyond Saturn remains essentially unknown. Clearly, a better understanding of how disk substructures form and how efficient they are in separating disk dust reservoirs is needed to link the formation of the CR chondrite reservoir to a specific region of the disk.

4.3. Distinct formation mechanism for CI chondrites

The CI chondrites stand out as the only carbonaceous chondrites whose Fe and Ni isotopic composition is unmatched by any of the differentiated CC meteorites. Spitzer et al. (2024) proposed that the distinct Fe and Ni isotopic composition of the CI chondrites reflect a more efficient accretion of small (*μm*-sized) FeNi metal grains, which are depleted in all other CC chondrites. These authors further suggested that these different efficiencies for incorporating FeNi metal grains reflect a distinct accretion mechanism for CI chondrites compared to the other CC chondrites; while formation of the latter involved dust pile-up in one or more pressure structure(s) of the disk, the CI chondrites formed by a distinct burst of planetesimal formation triggered by photoevaporation of the disk (Carrera et al., 2017). This mechanism is not tied to a specific region of the disk, and so would have caused planetesimal formation over a wide range of heliocentric distances. One key prediction of this model is that bodies with CI chondritic Fe and Ni isotopic compositions only formed late because dust enrichment by photoevaporation only occurred at the end of the disk's lifetime (Spitzer et al., 2024). Based on meteorite paleomagnetism, the lifetime of the solar gaseous disk is ~4 Ma (Wang et al., 2017), and so since at this time there was insufficient ^{26}Al remaining to trigger melting and differentiation of planetesimals (Hevey and Sanders, 2006), there should be no differentiated CC bodies having a CI chondrite-like Fe and Ni isotopic composition (Spitzer et al., 2024). This is consistent with our finding that none of the early-formed differentiated CC bodies have CI chondritic Fe and Ni isotopic compositions.

A different explanation for the distinct isotopic signature of CI compared to other CC chondrites is their formation in another spatially isolated reservoir, which may have been ice-rich and located beyond Saturn and potentially in the same region of the solar system as comets (Hopp et al., 2022a). In this model, the latter were ejected outwards to the Oort cloud by Uranus and Neptune, while CI chondrites were ejected inwards by the same process but through interaction with nebular gas were implanted into the main asteroid belt (Hopp et al., 2022a; Nesvorný et al., 2024). The CI chondrites may have lost their ice during passage close to the Sun on their originally highly elliptical orbits. Within this framework, the lack of differentiated bodies with CI-like Fe and Ni isotopic compositions could reflect that these bodies never differentiated because the presence of significant amounts of water ice (~30–50 wt. %) could have acted as a thermal buffer, absorbing heat released by ^{26}Al-decay as latent heat of melting and vaporization, dilution of the ^{26}Al mass fraction, and heat transport by migration of melted water (Grimm and McSween Jr., 1989). Models of planetesimal melting suggest that early-formed and icy planetesimals would only escape differentiation if they were small (radii ≤15 km) (Lichtenberg et al., 2021). Yet, the streaming instability naturally produces a power-law size distribution of planetesimals, meaning that most of the mass is concentrated in larger planetesimals (~100 km in diameter), but smaller objects are more numerous (Klahr and Schreiber, 2020). Thus, if the CI chondrites in our collections were to derive from such small, ice-rich, early-formed planetesimals, we would expect to also sample the larger CI-like planetesimals that formed alongside the smaller ones. This is because the larger objects have a higher chance of long-term survival due to their lower susceptibility to collisional destruction, inward migration, and dynamical ejection. However, these larger objects would likely have differentiated, even if they were rich in water ice (Lichtenberg et al., 2021). Consequently, the lack of differentiated meteorite parent bodies having CI-like Fe and Ni isotopic compositions is more readily accounted for if CI-like bodies formed late.

The late formation of CI chondrite-like bodies is also favored by our

current understanding of planetesimal formation. The streaming instability prefers pebbles with higher Stokes numbers, which is not only a function of the size and density of the dust grains but also the gas density (Youdin and Goodman, 2005). Thus, the formation of planetesimals rich in fine-grained material (like CI chondrites) is easier late in disk history when gas densities are lower. As CI chondrites represent agglomerates almost exclusively made of fine-grained dust, it seems unlikely that their formation via the streaming instability could have also been triggered <1 Ma after CAI formation (the time of iron meteorite parent body accretion) because the high gas density at that time would require these fine-grained dust grains to aggregate into larger dust agglomerates. Evaluating whether this was possible would require better knowledge of the sticking properties of such grains, which are poorly constrained (Blum, 2018). Altogether, these observations suggest that CI-like planetesimals accreted late in disk history, consistent with the idea that their formation was facilitated by gas removal during photoevaporation of the disk (Spitzer et al., 2024).

5. Conclusions

The same range of Fe and Ni isotopic compositions for early- (iron meteorites and achondrites) and late-formed (chondrites) CC-type planetesimals indicates that both generations of objects formed from similar mixtures of the same dust components (refractory inclusions, chondrule precursors, FeNi metal, and matrix). This is also true for the CR chondrites, which represent some of the latest CC planetesimals. However, many differentiated meteorites have a CR chondrite-like isotopic composition, indicating that this reservoir must have been established early and maintained for essentially the entire disk lifetime. In general, the recurrent formation of CC planetesimals for approximately 3–4 Ma suggests that there must have been an effective dust drift barrier that prevented the loss of these materials into the Sun. This barrier may have been a long-lived pressure structure in the disk in which both early and late CC planetesimals formed or was comprised of different substructures, which all contained the same dust components, albeit possibly in different proportions.

The CI chondrites are the only CC chondrites whose Fe and Ni isotopic compositions are not recorded in the early-formed differentiated meteorites, suggesting that planetesimals having CI-chondritic isotopic compositions only formed late. This is consistent with the idea that the CI chondrite parent bodies formed by a distinct accretion mechanism than other CC planetesimals and that their formation may have been triggered by the photoevaporative removal of the gas towards the end of the disk's lifetime (Spitzer et al., 2024). The origin of the uniquely distinct Fe and Ni isotopic compositions of the CI chondrites may be related to this different accretion mechanism (Spitzer et al., 2024) and/or reflects formation in a spatially separated reservoir of the disk in the outer regions of the solar system (Hopp et al., 2022a).

CRediT authorship contribution statement

Fridolin Spitzer: Writing – review & editing, Writing – original draft, Visualization, Investigation, Formal analysis, Data curation. **Timo Hopp:** Writing – review & editing, Investigation, Formal analysis, Data curation. **Christoph Burkhardt:** Writing – review & editing, Supervision, Project administration, Funding acquisition, Conceptualization. **Nicolas Dauphas:** Writing – review & editing, Supervision, Resources, Funding acquisition. **Thorsten Kleine:** Writing – review & editing, Resources, Project administration, Funding acquisition, Conceptualization.

Declaration of competing interest

The authors declare that they have no known competing financial interests or personal relationships that could have appeared to influence the work reported in this paper.

Acknowledgments

We thank the Field Museum Chicago, the National History Museum London, the Smithsonian Institution, the University of Mainz, and the Institut für Planetologie in Münster for generously providing meteorite samples for this study. Constructive comments by Bidong Zhang and Greg A. Brennecka, and efficient editorial handling by Olivier Mousis are greatly acknowledged. This project has been funded by the Deutsche Forschungsgemeinschaft (DFG, German Research Foundation) (Project-ID 263649064-TRR170). This is TRR publication #229. N. D. also acknowledges funding by NASA grants 80NSSC20K1409 (Habitable Worlds), 80NSSC23K1022 (LARS), 545 80NSSC21K0380 and 80NSSC20K0821 (Emerging Worlds), 80NSSC23K1163 (MMX-PSP), NSF grant EAR- (CSEDI), and DOE grant DE-SC0022451.

Supplementary material

Supplementary material associated with this article can be found, in the online version, at doi:10.1016/j.epsl.2025.119530.

Data availability

Data will be made available on request.

References

Alexander, C.M.O.D., 2019. Quantitative models for the elemental and isotopic fractionations in chondrites: the carbonaceous chondrites. Geochim. Cosmochim. Acta 254, 277–309. https://doi.org/10.1016/j.gca.2019.02.008.

Alexander, C.M.O.D., Bowden, R., Fogel, M.L., Howard, K.T., Herd, C.D.K., Nittler, L.R., 2012. The provenances of asteroids, and their contributions to the volatile inventories of the terrestrial planets. Science 337, 721–723. https://doi.org/10.1126/science.1223474.

Anand, A., Spitzer, F., Hopp, T., Windmill, R., Kruttasch, P., Burkhardt, C., Dauphas, N., Greenwood, R., Hofmann, B., Mezger, K., Kleine, T., 2024. Isotopic evidence for a common parent body of IIG and IIAB iron meteorites. Geochim. Cosmochim. Acta 382, 118–127. https://doi.org/10.1016/j.gca.2024.07.025.

Bai, X.N., Stone, J.M., 2010. The effect of the radial pressure gradient in protoplanetary disks on planetesimal formation. Astrophys. J. Lett. 722, L220. https://doi.org/10.1088/2041-8205/722/2/L220.

Bitsch, B., Morbidelli, A., Johansen, A., Lega, E., Lambrechts, M., Crida, A., 2018. Pebble-isolation mass: scaling law and implications for the formation of super-earths and gas giants. Astron. Astrophys. 612, A30. https://doi.org/10.1051/0004-6361/201731931.

Blum, J., 2018. Dust evolution in protoplanetary discs and the formation of planetesimals. Space Sci. Rev. 214, 52. https://doi.org/10.1007/s11214-018-0486-5.

Bollard, J., Connelly, J.N., Whitehouse, M.J., Pringle, E.A., Bonal, L., Jørgensen, J.K., Nordlund, Å., Moynier, F., Bizzarro, M., 2017. Early formation of planetary building blocks inferred from Pb isotopic ages of chondrules. Sci. Adv. 3, e1700407. https://doi.org/10.1126/sciadv.1700407.

Bryson, J.F.J., Brennecka, G.A., 2021. Constraints on chondrule generation, disk dynamics, and asteroid accretion from the compositions of carbonaceous meteorites. Astrophys. J. 912, 163. https://doi.org/10.3847/1538-4357/abea12.

Budde, G., Burkhardt, C., Brennecka, G.A., Fischer-Gödde, M., Kruijer, T.S., Kleine, T., 2016. Molybdenum isotopic evidence for the origin of chondrules and a distinct genetic heritage of carbonaceous and non-carbonaceous meteorites. Earth Planet. Sci. Lett. 454, 293–303. https://doi.org/10.1016/j.epsl.2016.09.020.

Budde, G., Burkhardt, C., Kleine, T., 2019. Molybdenum isotopic evidence for the late accretion of outer Solar System material to Earth. Nat. Astron. 3, 736–741. https://doi.org/10.1038/s41550-019-0779-y.

Budde, G., Kruijer, T.S., Kleine, T., 2018. Hf-W chronology of CR chondrites: implications for the timescales of chondrule formation and the distribution of ^{26}Al in the solar nebula. Geochim. Cosmochim. Acta 222, 284–304. https://doi.org/10.1016/j.gca.2017.10.014.

Burkhardt, C., Spitzer, F., Morbidelli, A., Budde, G., Render, J.H., Kruijer, T.S., Kleine, T., 2021. Terrestrial planet formation from lost inner solar system material. Sci. Adv. 7, eabj7601. https://doi.org/10.1126/sciadv.abj7601.

Carrera, D., Gorti, U., Johansen, A., Davies, M.B., 2017. Planetesimal formation by the streaming instability in a photoevaporating disk. Astrophys. J. 839, 16. https://doi.org/10.3847/1538-4357/aa6932.

Ciesla, F.J., 2007. Outward transport of high-temperature materials around the midplane of the solar nebula. Science 318, 613–615. https://doi.org/10.1126/science.1147273.

Connelly, J.N., Bizzarro, M., Krot, A.N., Nordlund, Å., Wielandt, D., Ivanova, M.A., 2012. The absolute chronology and thermal processing of solids in the solar protoplanetary disk. Science 338, 651–655. https://doi.org/10.1126/science.1226919.

Cook, D.L., Leya, I., Schönbächler, M., 2020. Galactic cosmic ray effects on iron and nickel isotopes in iron meteorites. Meteorit. Planet. Sci. 55, 2758–2771. https://doi.org/10.1111/maps.13446.

Dauphas, N., Hopp, T., Nesvorný, D., 2024. Bayesian inference on the isotopic building blocks of Mars and Earth. Icarus 408, 115805. https://doi.org/10.1016/j.icarus.2023.115805.

Desch, S.J., Kalyaan, A., Alexander, C.M.O., 2018. The effect of Jupiter's formation on the distribution of refractory elements and inclusions in meteorites. Astrophys. J. Suppl. Ser. 238, 11. https://doi.org/10.3847/1538-4365/aad95f.

Drążkowska, J., Alibert, Y., 2017. Planetesimal formation starts at the snow line. Astron. Astrophys. 608, A92. https://doi.org/10.1051/0004-6361/201731491.

Füri, E., Marty, B., 2015. Nitrogen isotope variations in the Solar System. Nat. Geosci. 8, 515–522. https://doi.org/10.1038/ngeo2451.

Goldstein, J.I., Scott, E.R.D., Chabot, N.L., 2009. Iron meteorites: crystallization, thermal history, parent bodies, and origin. Chem. Erde 69, 293–325. https://doi.org/10.1016/j.chemer.2009.01.002.

Grimm, R.E., McSween Jr., H.Y., 1989. Water and the thermal evolution of carbonaceous chondrite parent bodies. Icarus 82, 244–280. https://doi.org/10.1016/0019-1035(89)90038-9.

Hellmann, J.L., Hopp, T., Burkhardt, C., Kleine, T., 2020. Origin of volatile element depletion among carbonaceous chondrites. Earth Planet. Sci. Lett. 549, 116508. https://doi.org/10.1016/j.epsl.2020.116508.

Hellmann, J.L., Schneider, J.M., Wölfer, E., Drążkowska, J., Jansen, C.A., Hopp, T., Burkhardt, C., Kleine, T., 2023. Origin of isotopic diversity among carbonaceous chondrites. Astrophys. J. Lett. 946, L34. https://doi.org/10.3847/2041-8213/acc102.

Herzog, G.F., Caffee, M.W., 2014. Cosmic-Ray Exposure Ages of Meteorites, Meteorites and Cosmochemical Processes. Elsevier Ltd.

Hevey, P.J., Sanders, I.S., 2006. A model for planetesimal meltdown by ^{26}Al and its implications for meteorite parent bodies. Meteorit. Planet. Sci. 41, 95–106. https://doi.org/10.1111/j.1945-5100.2006.tb00195.x.

Hilton, C.D., Bermingham, K.R., Walker, R.J., McCoy, T.J., 2019. Genetics, crystallization sequence, and age of the South Byron Trio iron meteorites: new insights to carbonaceous chondrite (CC) type parent bodies. Geochim. Cosmochim. Acta 251, 217–228. https://doi.org/10.1016/j.gca.2019.02.035.

Hopp, T., Dauphas, N., Abe, Y., Aléon, J., O'D. Alexander, C.M., Amari, S., Amelin, Y., Bajo, K., Bizzarro, M., Bouvier, A., Carlson, R.W., Chaussidon, M., Choi, B.G., Davis, A.M., Di Rocco, T., Fujiya, W., Fukai, R., Gautam, I., Haba, M.K., Hibiya, Y., Hidaka, H., Homma, H., Hoppe, P., Huss, G.R., Ichida, K., Iizuka, T., Ireland, T.R., Ishikawa, A., Ito, M., Itoh, S., Kawasaki, N., Kita, N.T., Kitajima, K., Kleine, T., Komatani, S., Krot, A.N., Liu, M.C., Masuda, Y., McKeegan, K.D., Morita, M., Motomura, K., Moynier, F., Nakai, I., Nagashima, K., Nesvorný, D., Nguyen, A., Nittler, L., Onose, M., Pack, A., Park, C., Piani, L., Qin, L., Russell, S.S., Sakamoto, N., Schönbächler, M., Tafla, L., Tang, H., Terada, K., Terada, Y., Usui, T., Wada, S., Wadhwa, M., Walker, R.J., Yamashita, K., Yin, Q.Z., Yokoyama, T., Yoneda, S., Young, E.D., Yui, H., Zhang, A.C., Nakamura, T., Naraoka, H., Noguchi, T., Okazaki, R., Sakamoto, K., Yabuta, H., Abe, M., Miyazaki, A., Nakato, A., Nishimura, M., Okada, T., Yada, T., Yogata, K., Nakazawa, S., Saiki, T., Tanaka, S., Terui, F., Tsuda, Y., Watanabe, S., Yoshikawa, M., Tachibana, S., Yurimoto, H., 2022a. Ryugu's nucleosynthetic heritage from the outskirts of the Solar System. Sci. Adv. 8, 8141. https://doi.org/10.1126/sciadv.add8141.

Hopp, T., Dauphas, N., Spitzer, F., Burkhardt, C., Kleine, T., 2022b. Earth's accretion inferred from iron isotopic anomalies of supernova nuclear statistical equilibrium origin. Earth Planet. Sci. Lett. 577, 117245. https://doi.org/10.1016/j.epsl.2021.117245.

Izidoro, A., Dasgupta, R., Raymond, S.N., Deienno, R., Bitsch, B., Isella, A., 2022. Planetesimal rings as the cause of the Solar System's planetary architecture. Nat. Astron. 6, 357–366. https://doi.org/10.1038/s41550-021-01557-z.

Klahr, H., Schreiber, A., 2020. Turbulence sets the length scale for planetesimal formation: local 2D simulations of streaming instability and planetesimal formation. Astrophys. J. 901, 54. https://doi.org/10.3847/1538-4357/abac58.

Kleine, T., Mezger, K., Palme, H., Scherer, E., Münker, C., 2005. Early core formation in asteroids and late accretion of chondrite parent bodies: evidence from ^{182}Hf-^{182}W in CAIs, metal-rich chondrites, and iron meteorites. Geochim. Cosmochim. Acta 69, 5805–5818. https://doi.org/10.1016/j.gca.2005.07.012.

Krot, A.N., Bizzarro, M., 2009. Chronology of meteorites and the early solar system. Geochim. Cosmochim. Acta, The Chronology of Meteorites and the Early Solar System 73, 4919–4921. https://doi.org/10.1016/j.gca.2009.04.039.

Kruijer, T.S., Burkhardt, C., Budde, G., Kleine, T., 2017. Age of Jupiter inferred from the distinct genetics and formation times of meteorites. In: Proc. Natl. Acad. Sci. U. S. A., 114, pp. 6712–6716. https://doi.org/10.1073/pnas.1704461114.

Kruijer, T.S., Fischer-Gödde, M., Kleine, T., Sprung, P., Leya, I., Wieler, R., 2013. Neutron capture on Pt isotopes in iron meteorites and the Hf-W chronology of core formation in planetesimals. Earth Planet. Sci. Lett. 361, 162–172. https://doi.org/10.1016/j.epsl.2012.10.014.

Kruijer, T.S., Touboul, M., Fischer-Gödde, M., Bermingham, K.R., Walker, R.J., Kleine, T., 2014. Protracted core formation and rapid accretion of protoplanets. Science 344, 1150–1154. https://doi.org/10.1126/science.1251766.

Lichtenberg, T., Drazkowska, J., Schönbächler, M., Golabek, G.J., Hands, T.O., 2021. Bifurcation of planetary building blocks during Solar System formation. Science 371, 365–370. https://doi.org/10.1126/science.abb3091.

Luu, T.H., Hin, R.C., Coath, C.D., Elliott, T., 2019. Bulk chondrite variability in mass independent magnesium isotope compositions – Implications for initial solar system 26Al/27Al and the timing of terrestrial accretion. Earth Planet. Sci. Lett. 522, 166–175. https://doi.org/10.1016/j.epsl.2019.06.033.

Ma, N., Neumann, W., Néri, A., Schwarz, W.H., Ludwig, T., Trieloff, M., Klahr, H., Bouvier, A., 2022. Early formation of primitive achondrites in an outer region of the protoplanetary disc. Geochem. Perspect. Lett. 23, 33–37. https://doi.org/10.7185/geochemlet.2234.

Marrocchi, Y., Jones, R.H., Russell, S.S., Hezel, D.C., Barosch, J., Kuznetsova, A., 2024. Chondrule properties and formation conditions. Space Sci. Rev. 220, 69. https://doi.org/10.1007/s11214-024-01102-0.

Marrocchi, Y., Piralla, M., Regnault, M., Batanova, V., Villeneuve, J., Jacquet, E., 2022. Isotopic evidence for two chondrule generations in CR chondrites and their relationships to other carbonaceous chondrites. Earth Planet. Sci. Lett. 593, 117683. https://doi.org/10.1016/J.EPSL.2022.117683.

Morbidelli, A., Baillié, K., Batygin, K., Charnoz, S., Guillot, T., Rubie, D.C., Kleine, T., 2022. Contemporary formation of early Solar System planetesimals at two distinct radial locations. Nat. Astron. 6, 72–79. https://doi.org/10.1038/s41550-021-01517-7.

Nesvorný, D., Dauphas, N., Vokrouhlický, D., Deienno, R., Hopp, T., 2024. Isotopic trichotomy of main belt asteroids from implantation of outer solar system planetesimals. Earth Planet. Sci. Lett. 626, 118521. https://doi.org/10.1016/j.epsl.2023.118521.

Nie, N.X., Chen, X.Y., Hopp, T., Hu, J.Y., Zhang, Z.J., Teng, F.Z., Shahar, A., Dauphas, N., 2021. Imprint of chondrule formation on the K and Rb isotopic compositions of carbonaceous meteorites. Sci. Adv. 7, 3929. https://doi.org/10.1126/sciadv.abl3929.

Olsen, M.B., Wielandt, D., Schiller, M., Van Kooten, E.M.M.E., Bizzarro, M., 2016. Magnesium and 54Cr isotope compositions of carbonaceous chondrite chondrules – Insights into early disk processes. Geochim. Cosmochim. Acta 191, 118–138. https://doi.org/10.1016/j.gca.2016.07.011.

Piani, L., Marrocchi, Y., Vacher, L.G., Yurimoto, H., Bizzarro, M., 2021. Origin of hydrogen isotopic variations in chondritic water and organics. Earth Planet. Sci. Lett. 567, 117008. https://doi.org/10.1016/j.epsl.2021.117008.

Piralla, M., Villeneuve, J., Schnuriger, N., Bekaert, D.V., Marrocchi, Y., 2023. A unified chronology of dust formation in the early solar system. Icarus 394, 115427. https://doi.org/10.1016/J.ICARUS.2023.115427.

Pringle, E.A., Moynier, F., Beck, P., Paniello, R., Hezel, D.C., 2017. The origin of volatile element depletion in early solar system material: clues from Zn isotopes in chondrules. Earth Planet. Sci. Lett. 468, 62–71. https://doi.org/10.1016/J.EPSL.2017.04.002.

Sanborn, M.E., Wimpenny, J., Williams, C.D., Yamakawa, A., Amelin, Y., Irving, A.J., Yin, Q.Z., 2019. Carbonaceous achondrites Northwest Africa 6704/6693: milestones for early Solar System chronology and genealogy. Geochim. Cosmochim. Acta 245, 577–596. https://doi.org/10.1016/j.gca.2018.10.004.

Schrader, D.L., Nagashima, K., Krot, A.N., Ogliore, R.C., Yin, Q.Z., Amelin, Y., Stirling, C.H., Kaltenbach, A., 2017. Distribution of 26Al in the CR chondrite chondrule-forming region of the protoplanetary disk. Geochim. Cosmochim. Acta, Isotopic studies of planetary and nuclear materials: A scientific tribute to Ian Douglass Hutcheon (1947-2015) 201, 275–302. https://doi.org/10.1016/j.gca.2016.06.023.

Scott, E.R.D., Krot, A.N., 2013. Chondrites and Their Components, Treatise on Geochemistry, 2nd Edition. Elsevier Ltd. https://doi.org/10.1016/B978-0-08-095975-7.00104-2.

Spitzer, F., Burkhardt, C., Budde, G., Kruijer, T.S., Morbidelli, A., Kleine, T., 2020. Isotopic evolution of the inner solar system inferred from molybdenum isotopes in meteorites. Astrophys. J. Lett. 898, L2. https://doi.org/10.3847/2041-8213/ab9e6a.

Spitzer, F., Burkhardt, C., Kruijer, T.S., Kleine, T., 2025. Comparison of the earliest NC and CC planetesimals: evidence from ungrouped iron meteorites. Geochim. Cosmochim. Acta 397, 134–148. https://doi.org/10.1016/j.gca.2025.03.021.

Spitzer, F., Burkhardt, C., Nimmo, F., Kleine, T., 2021. Nucleosynthetic Pt isotope anomalies and the Hf-W chronology of core formation in inner and outer solar system planetesimals. Earth Planet. Sci. Lett. 576, 117211. https://doi.org/10.1016/j.epsl.2021.117211.

Spitzer, F., Burkhardt, C., Pape, J., Kleine, T., 2022. Collisional mixing between inner and outer solar system planetesimals inferred from the Nedagolla iron meteorite. Meteorit. Planet. Sci. 57, 261–276. https://doi.org/10.1111/maps.13744.

Spitzer, F., Kleine, T., Burkhardt, C., Hopp, T., Yokoyama, T., Abe, Y., Aléon, J., O'D Alexander, C.M., Amari, S., Amelin, Y., Bajo, K., Bizzarro, M., Bouvier, A., Carlson, R.W., Chaussidon, M., Choi, B.G., Dauphas, N., Davis, A.M., Di Rocco, T., Fujiya, W., Fukai, R., Gautam, I., Haba, M.K., Hibiya, Y., Hidaka, H., Homma, H., Hoppe, P., Huss, G.R., Ichida, K., Iizuka, T., Ireland, T.R., Ishikawa, A., Itoh, S., Kawasaki, N., Kita, N.T., Kitajima, K., Komatani, S., Krot, A.N., Liu, M.C., Masuda, Y., Morita, M., Moynier, F., Motomura, K., Nakai, I., Nagashima, K., Nguyen, A., Nittler, L., Onose, M., Pack, A., Park, C., Piani, L., Qin, L., Russell, S.S., Sakamoto, N., Schönbächler, M., Tafla, L., Tang, H., Terada, K., Terada, Y., Usui, T., Wada, S., Wadhwa, M., Walker, R.J., Yamashita, K., Yin, Q.Z., Yoneda, S., Young, E.D., Yui, H., Zhang, A.C., Nakamura, T., Naraoka, H., Noguchi, T., Okazaki, R., Sakamoto, K., Yabuta, H., Abe, M., Miyazaki, A., Nakato, A., Nishimura, M., Okada, T., Yada, T., Yogata, K., Nakazawa, S., Saiki, T., Tanaka, S., Terui, F., Tsuda, Y., Watanabe, S., Yoshikawa, M., Tachibana, S., Yurimoto, H., 2024. The Ni isotopic composition of Ryugu reveals a common accretion region for carbonaceous chondrites. Sci. Adv. 10, eadp2426. https://doi.org/10.1126/sciadv.adp2426.

Tomkins, A.G., Johnson, T.E., Mitchell, J.T., 2020. A review of the chondrite–achondrite transition, and a metamorphic facies series for equilibrated primitive stony meteorites. Meteorit. Planet. Sci. 55, 857–885. https://doi.org/10.1111/maps.13472.

Van Kooten, E.M.M.E., Cavalcante, L., Wielandt, D., Bizzarro, M., 2020. The role of bells in the continuous accretion between the CM and CR chondrite reservoirs. Meteorit. Planet. Sci. 55, 575–590. https://doi.org/10.1111/maps.13459.

Van Kooten, E.M.M.E., Wielandt, D., Schiller, M., Nagashima, K., Thomen, A., Larsen, K. K., Olsen, M.B., Nordlund, Å., Krot, A.N., Bizzarro, M., 2016. Isotopic evidence for primordial molecular cloud material in metal-rich carbonaceous chondrites. Proc. Natl. Acad. Sci. U. S. A. 113, 2011–2016. https://doi.org/10.1073/pnas.1518183113.

Van Kooten, E.M.M.E., Zhao, X., Franchi, I., Tung, P.Y., Fairclough, S., Walmsley, J., Onyett, I., Schiller, M., Bizzarro, M., 2024. The nucleosynthetic fingerprint of the outermost protoplanetary disk and early Solar System dynamics. Sci. Adv. 10, eadp1613. https://doi.org/10.1126/sciadv.adp1613.

Villeneuve, J., Chaussidon, M., Libourel, G., 2009. Homogeneous distribution of ^{26}Al in the solar system from the Mg isotopic composition of chondrules. Science 325, 985–988. https://doi.org/10.1126/science.1173907.

Wang, H., Weiss, B.P., Bai, X.N., Downey, B.G., Wang, Jun, Wang, Jiajun, Suavet, C., Fu, R.R., Zucolotto, M.E., 2017. Lifetime of the solar nebula constrained by meteorite paleomagnetism. Science 355, 623–627. https://doi.org/10.1126/science.aaf5043.

Warren, P.H., 2011. Stable-isotopic anomalies and the accretionary assemblage of the Earth and Mars: a subordinate role for carbonaceous chondrites. Earth Planet. Sci. Lett. 311, 93–100. https://doi.org/10.1016/j.epsl.2011.08.047.

Williams, C.D., Sanborn, M.E., Defouilloy, C., Yin, Q.Z., Kita, N.T., Ebel, D.S., Yamakawa, A., Yamashita, K., 2020. Chondrules reveal large-scale outward transport of inner Solar System materials in the protoplanetary disk. In: Proc. Natl. Acad. Sci., 117, pp. 23426–23435. https://doi.org/10.1073/pnas.2005235117.

Wittig, N., Humayun, M., Brandon, A.D., Huang, S., Leya, I., 2013. Coupled W-Os-Pt isotope systematics in IVB iron meteorites: in situ neutron dosimetry for W isotope chronology. Earth Planet. Sci. Lett. 361, 152–161. https://doi.org/10.1016/j.epsl.2012.10.013.

Wölfer, E., Budde, G., Kleine, T., 2023. Age and genetic relationships among CB, CH and CR chondrites. Geochim. Cosmochim. Acta 361, 288–301. https://doi.org/10.1016/j.gca.2023.10.010.

Wölfer, E., Burkhardt, C., Nimmo, F., Kleine, T., 2025. Origin of moderately volatile elements in Earth inferred from mass-dependent Ge isotope variations among chondrites. Earth Planet. Sci. Lett. 663, 119435. https://doi.org/10.1016/j.epsl.2025.119435.

Yang, L., Ciesla, F.J., 2012. The effects of disk building on the distributions of refractory materials in the solar nebula. Meteorit. Planet. Sci. 47, 99–119. https://doi.org/10.1111/j.1945-5100.2011.01315.x.

Yap, T.E., Tissot, F.L.H., 2023. The NC-CC dichotomy explained by significant addition of CAI-like dust to the Bulk Molecular Cloud (BMC) composition. Icarus 405, 115680. https://doi.org/10.1016/j.icarus.2023.115680.

Youdin, A.N., Goodman, J., 2005. Streaming instabilities in protoplanetary disks. Astrophys. J. 620, 459–469. https://doi.org/10.1086/426895.